RSC Advances

PAPER

View Article Online
View Journal | View Issue

Cite this: *RSC Adv.*, 2025, **15**, 29254

Self-healing quercetin loaded hyaluronic dialdehyde conjugated aminoethyl-β-cyclodextrin and chitosan hydrogel *via* Schiff base reaction for enhanced anti-inflammatory activity

Parichat Sutthisawatkul,[a] Kanyalux Stapornpiriyadaj,[a] Onuma Mongkhon,[a] Weerasak Taengphan,[b] Theerachart Leepasert[a] and Thitinun Karpkird *[a]

In this work, hydrogels composed of hyaluronic dialdehyde (HAD) and amino-beta-cyclodextrin (ACD) incorporated with quaternary ammonium chitosan (HACC) were synthesized *in situ via* Schiff base reaction. The composition, morphology and mechanical properties were characterized using FTIR, ^{1}H-NMR, SEM and rheological testing. Hydrogels were prepared using different molecular weights of HAD. The results showed that a higher molecular weight of HAD has increased the swelling ratio up to 1715–1835% and enhanced the mechanical properties of hydrogels. Increasing the HAD content further improved stability and mechanical properties due to a higher degree of crosslinking. Quercetin (Que), was used as a hydrophobic drug to form an inclusion complex with ACD and was loaded in HAD-ACD-HACC hydrogels. Drug release, cytotoxicity and anti-inflammatory activity were investigated *in vitro*. The results indicated that quercetin release was higher in acidic media than in neutral solutions. Cellular assessment of quercetin loaded 100k-2 and 1M-2 hydrogels by scratch test encouraged the migration of human keratinocyte (HaCaT) cells. The anti-inflammatory activity of quercetin loaded 100k-2 hydrogel was improved compared to free quercetin against HaCaT cells. Thus, this quercetin-loaded hydrogel system offers a promising approach for controlled drug release, enhanced anti-inflammatory and wound healing activities in various biomedical applications.

Received 12th May 2025
Accepted 11th August 2025

DOI: 10.1039/d5ra03329b

rsc.li/rsc-advances

1. Introduction

Quercetin (Que), is a flavonoid found in many common fruits and vegetables. It is a potent scavenger of reactive oxygen species and has neuroprotective effects.[1] Quercetin is also reported to reduce the secretion of pro-inflammatory factors like nitric oxide (NO), and pro-inflammatory cytokines such as interleukin-6 (IL-6), tumor necrosis factor-α (TNF-α), and prostaglandin E2 (PGE2).[2] Interleukin-6 (IL-6) is released by macrophages responding to an injury or a specific microbial molecule, inducing fever. Quercetin is reported to decrease the production of inflammatory mediators, including IL-6, NO and PGE2 by interfering with the response of cells to pro-inflammatory factors.[2,3] However, quercetin has low solubility and bioavailability, limiting its pharmaceutical applications,[4,5] thereby necessitating the development of an effective delivery system that can enhance its solubility, protect it from degradation, and ensure sustained and targeted release. Hydrogels are polymeric materials that are hydrated and highly cross-linked in a three-dimensional structure, exhibiting high elasticity and the ability to swell or collapse depending on their hydration level.[6] Their advantageous properties, such as superior hydrophilicity, biocompatibility, and mechanical strength similar to biological soft tissues and bio-adhesives, make them suitable for applications such as sustained drug release, drug and cell delivery, wound dressing, tissue engineering and targeted cancer therapy.[7,8] Various hydrogel structures have been developed for the sustained delivery of small active compounds, proteins, peptides, or nucleic acids, utilizing biopolymers such as hyaluronic acid, chitosan, alginate, gelatin, collagen, cellulose and their derivatives.[9–13] Among various hydrogel forming materials, hyaluronic acid (HA) stands out, given that it's naturally found in the human body.[14] It exhibits excellent moisturizing properties, biocompatibility, biodegradability and gelation ability. Moreover, HA is a ubiquitous component of the extracellular matrix (ECM).[15] However, the mechanical properties of hydrogels containing only HA are insufficient.[16] To address this limitation, HA can be crosslinked using various physical and chemical methods, making it a promising biomaterial for applications in tissue engineering, drug delivery, and wound healing.[17,18] Chitosan (CS) is a natural cationic polysaccharide derived from chitin, containing a large number of amino groups, and is widely used in

[a]*Department of Chemistry, Faculty of Science, Kasetsart University, Chatuchak, Bangkok, 10900, Thailand. E-mail: fscitnm@ku.ac.th*

[b]*Expert Center of Innovative Herbal Products, Thailand Institute of Scientific and Technological Research, Khlong Luang, Pathum Thani, Thailand*

wound healing applications. CS is an excellent candidate for biomedical applications and tissue engineering due to its cytocompatibility, non-allergenicity, biodegradability, mucoadhesiveness, antioxidant properties, and antibacterial properties.[13] Chitosan quaternary ammonium salt, known as hydroxypropyltrimethyl ammonium chloride chitosan (HACC), is a quaternized chitosan derivative has been developed to enhance these properties. HACC-based hydrogels are typically prepared through ionic crosslinking, hydrogen bond crosslinking, and chemical crosslinking.[19] Hydrogels with chemical cross-linking are formed by a covalent bond that can be activated by chemical reaction or light. These types of hydrogels generate a stronger bond and exhibit greater heat stability.[20,21] There are many cross-linking reaction typed and reactivity of the reactants in the formulation such as, esterification reaction, Michael type addition, and Schiff base reaction. The Schiff base reaction is preferred due to the rapid formation, occurring spontaneously at room temperature, and the unnecessary addition of external crosslinkers.[22–24] Furthermore, this cross-linked type can decompose in acidic and basic conditions. Therefore, it could be safe for use in terms of drug-delivery through human skin.[25,26] To further improve the drug-loading efficiency and molecular stability of hydrophobic drugs like quercetin, cyclodextrins (CDs) have been extensively employed. β-Cyclodextrin (β-CD) is a cyclic oligosaccharide consisting of seven glucose units linked by 1,4-α-glucosidic bond. It features a hydrophilic exterior and hydrophobic inner cavity, allowing for the encapsulation of hydrophobic molecules. Oxidized dextran and hydrazine-functionalized polyaspartamide with CD and PEG moieties were used to form the hydrogel *via* a Schiff-base reaction. The characteristics and properties of this system were tunable by adjusting the crosslinking density.[27–30] Many studies reported that crosslinking of hyaluronic acid and cyclodextrin is constructed using permanent covalent bonds, which are not reversible. The oxidation of beta-cyclodextrin to dialdehyde, followed by its reaction with amino-functionalized hyaluronic acid or chitosan, has been widely reported.[31–33] However, the oxidation of cyclodextrin to dialdehyde may lead to breaking the CD cavity and loss of its cyclodextrin properties.[34]

To retain the encapsulation ability of CD, in this work, a novel hydrogel system was developed using hyaluronic acid dialdehyde (HAD) conjugated with amino-beta-cyclodextrin (ACD) *via* Schiff base linkage (Fig. 1). Quaternary ammonium chitosan (HACC) was incorporated to stabilize the gelation of the hydrogel system. The hypothesis of this study is that quercetin-loaded HAD:ACD:HACC hydrogels can control drug release through hydrolysis of imine linkages under acidic conditions and enhance anti-inflammatory activity through the formation of an inclusion complex with ACD. The effect of the different molecular weights of HAD on mechanical properties and swelling ratio was investigated. This system demonstrates great potential as a promising biomaterial for advanced wound healing and skin regeneration applications.

2. Materials and methods

2.1 Materials

Four sizes of hyaluronic acid, HA10k (M_w 10 000 Da), HA100k (M_w 8000–50 000 Da), HA1M (M_w 80 000–1 500 000 kDa) and HA2M (M_w 1 800 000–2 500 000 Da) were purchased from Chanjao Longevity (Bangkok). *N*-(2-Hydroxy)propyl-3-trimentylammonium chitosan chloride (HACC, 70 kDa, degree of quaternization 46%, degree of deacetylation 90%, purity: pharmaceutical grade) was purchased from Chanjao Longevity (Bangkok). *β*-Cyclodextrin (>99.0%) and ethylenediamine (EDA) were purchased from Tokyo Chemical Industry (TCI). Sodium periodate was purchased from Loba Chemie. Ethylene glycol was purchased from Supelco®. *p*-Thiosulfonyl chloride (TsCl) was purchased from Sigma-Aldrich. Sodium hydroxide was purchased from Emsure®. Hydrochloric acid and all solvents were purchased from RCI Labscan Ltd (Bangkok).

2.2 Synthesis

2.2.1 Synthesis of hyaluronic acid dialdehyde (HAD). HAD was synthesized accordance to the literature.[35] Briefly, 2.0 g of HA was dissolved in 100 mL of distilled water. A solution of 0.586 g of $NaIO_4$ in 15 mL of distilled water was slowly added, and the mixture was stirred at room temperature for 24 h. Ethylene glycol (2 mL) was added to stop the reaction, and the mixture was stirred continuously for 1 h. For purification, the mixture was dialyzed (MWCO 14 kDa) against distilled water at least three times/day for three days and lyophilized to obtain a white solid. The oxidation degree of HAD is analyzed by the ratio of integration of the ^{1}H-NMR signal of aldehyde protons and methyl of the acetyl group of HAD.

2.2.2 Synthesis of mono-(6-tosyl-6-deoxy)-beta-cyclodextrin (bCDTs). The synthesis of bCDTs was performed according to the literature.[36] Firstly, 5.0 g of β-CD was suspended in 35 mL of water and, 5 mL of 0.01 M NaOH was added dropwise over 5 min. The mixture was reacted under vigorous agitation at 0 °C for 1 h, then 0.84 g of *p*-toluenesulfonyl chloride (TsCl) in 20 mL of acetonitrile was added dropwise over 15 min. After 1 h of stirring at room temperature, unreacted TsCl was filtered off, the solution was neutralized with a pH of 7–8 by 1 M hydrochloric acid, and the filtrate was refrigerated overnight at 4 °C. The white precipitate was recovered by suction filtration and recrystallized in water at least three times. The sample obtained was dried in a desiccator for 24 h, and bCDTs were obtained as a white solid.

2.2.3 Synthesis of mono-(6-ethanediamine-6-deoxy)-beta-cyclodextrin (ACD). ACD was synthesized by modification of the literature.[37] Briefly, 1.0 g of bCDTs was reacted with an excess amount of EDA (6 mL) in 20 mL DMF at 80 °C for 6 h. After the mixture was allowed to cool to room temperature, 8 mL of cold methanol was added, and the mixture was slowly precipitated with acetone. To purify, the precipitate was repeatedly dissolved in water and precipitated with acetone three times for the removal of unreacted EDA. The white solid of ACD was dried at room temperature for 24 h in a desiccator.

2.3 Preparation of HAD-ACD-HACC crosslinked hydrogels

Stock solutions of 1% w/v HAD and 6% w/v ACD were prepared in water. The solution of 2% w/v HACC was prepared in 1% acetic acid. The different ratios of HAD-ACD-HACC hydrogels were prepared (with the mole ratio 1-2-10 and 2-2-10) *via* rapidly and fully mixing the above solutions at room temperature. The

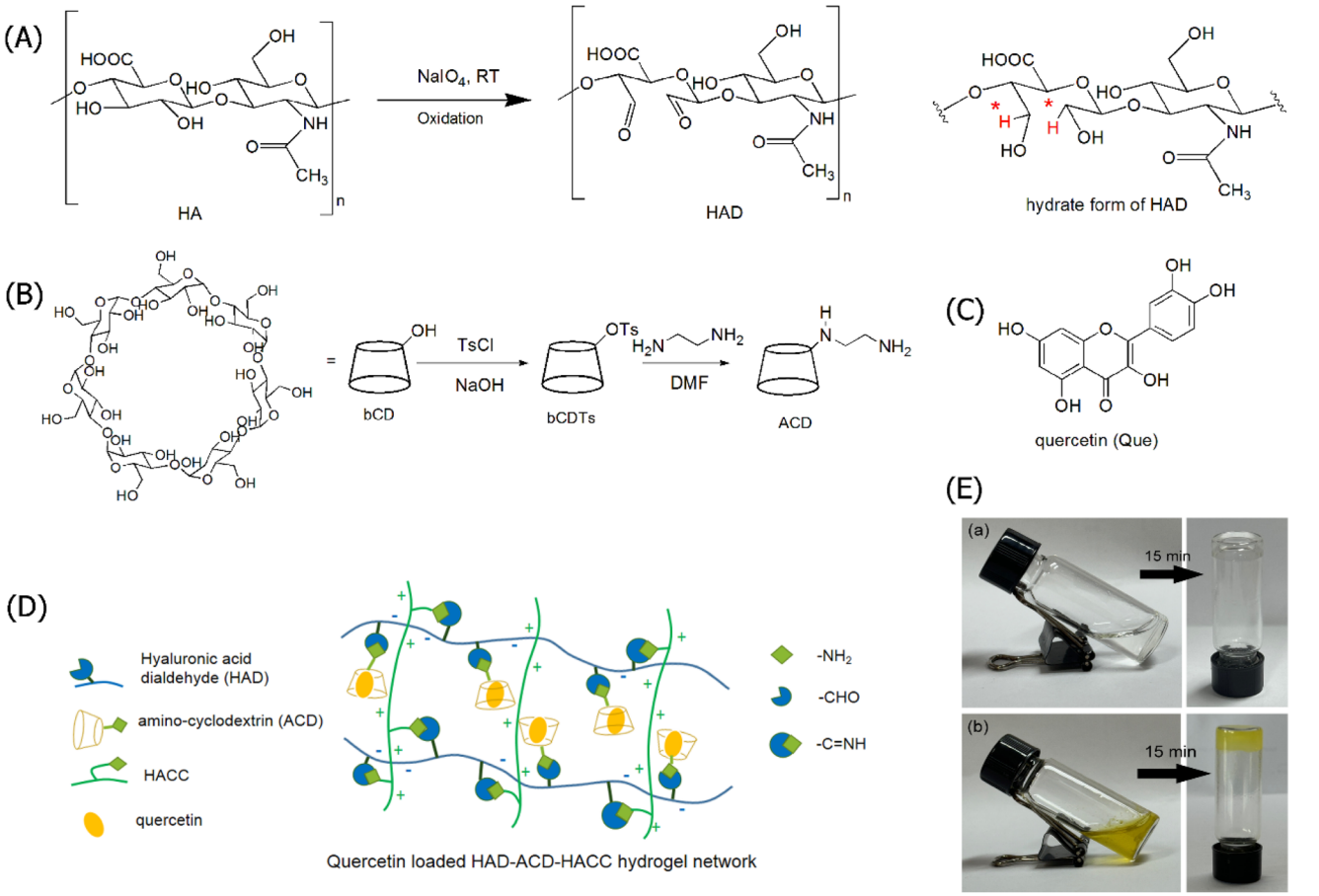

Fig. 1 Schematic illustration of chemical structure and synthesis pathway of HAD (A), ACD (B), quercetin (C) quercetin loaded HAD-ACD-HACC Schiff base hydrogel network (D) and visual observation of hydrogel formation for 100k-2 (top) and Q100k-2 (bottom) gelling solution (E).

pH of the solution mixture was adjusted to 7.4 with PBS. The solution mixtures were left at room temperature to form a gel.

2.4 Preparation of quercetin (Que) loaded HAD-ACD-HACC hydrogels

The active compound, quercetin (Que), was dissolved in ethanol and added to the ACD solution at a ratio of 1 : 1 Que : ACD. The mixture was stirred at room temperature in the dark for 24 h to allow ethanol evaporation, followed by centrifugation to separate free Que. A clear solution of the Que:ACD inclusion complex was obtained and lyophilized. The dry Que:ACD inclusion complex used in the next step to form the hydrogel follows the method described above.

The concentration of Que in the inclusion complex is calculated by using UV absorption spectrometry, compared to a quercetin standard curve. The loading capacity (LC) of Que in Que:ACD inclusion complex was calculated using eqn (1). The experiment was done in triplicate.

$$\%\ \mathrm{LC} = (W_{\mathrm{Q}}/W_{\mathrm{Quecpx}}) \times 100 \quad (1)$$

where W_{Q} represents the weight of Que loaded into the inclusion complex, W_{Quecpx} represents the weight of Que:ACD inclusion complex.

The encapsulation efficiency (% EE) of quercetin loaded in HAD-ACD-HACC hydrogel was calculated using eqn (2). The experiment was done in triplicate.

$$\%\ \mathrm{EE} = (W_{\mathrm{Qgel}}/W_{\mathrm{Quecpx}}) \times 100 \quad (2)$$

where W_{Qgel} represents the weight of Que loaded in hydrogel and W_{Quecpx} represents weight of quercetin in the Que:ACD inclusion complex added into the formulation.

2.5 Characterization methods

HAD and ACD as well as HAD-ACD-HACC hydrogels were analyzed using ^{1}H-NMR spectroscopy (Brucker 400 MHz AVANCE III HD spectrometer operating at 400 MHz) and Fourier-Transform Infrared spectrometer Fourier Transform Infrared spectroscopy (FT-IR) (PerkinElmer, Spectrum II). The internal morphology of hydrogels will be observed through a scanning electron microscope (SEM), after lyophilized, fractured in liquid nitrogen, and sprayed with gold for 100 s.

2.6 Rheological analysis of hydrogel structures

The storage modulus (G') and loss modulus (G'') of hydrogels were detected at 37 °C, dynamic oscillation scanning frequency

1–100 Hz, strain set as 100% by rotary rheometer (Brookfield DV III).

2.7 Swelling study

A piece of hydrogel was weighted (W_d) and immersed in DI water for 1 h, then the swellen hydrogel was weighted (W_s). The swelling ratio was calculated according to the following eqn (3). All samples were done in triplicate.

$$\text{Swelling ratio (\%)} = [(W_s - W_d)/W_d] \times 100\% \quad (3)$$

2.8 Releasing of quercetin study

The Quegel was placed into a dialysis membrane and immersed in 5 mL of PBS buffer (pH 7.4 and 5) at a temperature of 37 °C. Subsequently, at scheduled intervals, 200 μL of solution was withdrawn and replaced with the same volume of fresh buffer. The amount of Que released was detected by UV-vis spectrometry at $\lambda = 330$ nm and calculated from a quercetin calibration curve. All measurements were done in triplicate.

2.9 Cytotoxic study

Cell viability was determined using WST-1 assay to estimate the probable cytotoxic effect of the test compound and positive controls (0.1% sodium dodecyl sulphate, SDS) on human keratinocyte cells (HaCaT; CLS-300493; CLS, Germany). The number of viable cells was determined by the ability of mitochondria to convert tetrazolium salt WST-1 to a WST-1 water-soluble formazan. The amount of a water-soluble formazan generated by dehydrogenase in a cell is directly proportional to the number of viable cells present and can be measured spectrophotometrically. Briefly, the HaCaT cells were cultured and maintained in Dulbecco' s Modified Eagle Medium (DMEM) containing 10% heat-inactivated fetal bovine serum (FBS) and 1% penicillin-streptomycin in a humidified atmosphere incubator with 5% CO_2 at 37 °C. When the cell density from reaching 80% of culture flask, the remaining adherent cells were trypsinized for 5 min, counted by a hemocytometer, and seeded with 100 μL into 96-well plates at 2×10^5 cells per mL, then incubated overnight. The cells were then treated with each sample at various concentrations for 24 h. After incubation, 100 μL of WST-1 solution (Abcam, USA) was replaced prior to incubation at 37 °C for 30 min before measuring the absorbance at 450 nm in a microplate reader (TECAN, Infinite M200 PRO, USA). All experiments were done in triplicate. Cell viability was calculated using the following formula:

$$\text{Cell viability (\%)} = (\text{absorbance of treated cells/absorbance of untreated cells}) \times 100$$

2.10 Anti-inflammatory activity study

HaCaT cells were seeded at 5×10^5 cells per mL in 24-well plates. Cells were then incubated for 24 h with samples and 100 μg mL^{-1} of D,L-1′-acetoxychavicol acetate (DL-1) or β-glucan as positive controls. After that, the cells in each well were washed and replaced with PBS. The UV stimulation process was performed by the exposure to UVA (314–400 nm, 3.0 W) and UVB (280–315 nm, 13.6 W) for 22 s. Then, PBS was replaced with media and further incubated for 24 h. After incubation, the cell culture supernatants were quantified as an indicator of inflammatory cytokine production *via* an enzyme-linked immunosorbent assay (ELISA). Absorbance was read at 450 nm with a microplate reader, and all standards and samples were assayed in triplicate.

2.11 Scratch wound healing assay

Wound healing and migration assays are done by seeding HaCaT cells at a cell density of 2×10^4 cells per mL containing Dulbecco's modified Eagle's medium culture medium supplemented with 10% fetal bovine serum (FBS) into the Culture-Insert 2 Well (ibidi GmbH, Gräfelfing, Germany) in 24 well plate and incubated overnight at 37 °C in a humidified 5% CO_2 atmosphere for 24 hours. After cell attachment, a cell-free gap is created in which the cell migration can be visualized. The DMEM was completely removed and washed with PBS. Then, the cells were treated with the samples (1.25 mg mL^{-1}, each). Control cells received only fresh DMEM. The cells were then incubated at 37 °C in humidified 5% CO_2 atmosphere. The gap area was recorded at 24, 48 and 72 hours in a comparison with the initial gap size at 0 hours with the inverted microscope (ZEISS Axio Vert.A1, Carl Zeiss Microscopy, USA) (20× magnification) and calculated as the gap area. The wound healing rate was calculated as following;

$$\text{Wound healing (\%)} = [(\text{initial gap area} - \text{gap area time interval})/\text{initial gap area}] \times 100$$

2.12 Statistical analysis

Statistical comparisons were carried out by Tukey's Honestly Significant Test. All quantitative results are presented as mean ± SEM. Statistical significance was defined as a P value less than 0.05 ($P < 0.05$).

3. Results and discussion

3.1 Synthesis and characterization of HAD and ACD

HAD was obtained by oxidizing vicinal glycol in the glucopyranoside unit of hyaluronic acid using $NaIO_4$ as shown in Fig. 1a. The sizes of HA used in this work were 10k, 100k, 1M and 2M daltons. The amount of $NaIO_4$ and reaction time were varied as shown in Table 1. The results showed that oxidation degree (% OD) increased to over 90% when the amount of $NaIO_4$ was increased to 2.0 equivalents and the reaction time to 24 h. Therefore, the optimized condition used for further HAD synthesis for all experiments in this work was 2.0 equivalents of $NaIO_4$ and 24 h reaction time. The % OD can be determined by comparing the integration of the methyl of acetyl group of HA

and hemiacetal protons, which is a hydrate form of aldehyde groups from ^{1}H-NMR (Fig. 2).

The structure of HAD was characterized by ^{1}H-NMR and FT-IR (Fig. 2 and S1). The ^{1}H-NMR signals appeared at 4.9–5.3 ppm corresponding to the hemiacetal group, which was due to the hydrate form of aldehyde groups. FT-IR spectra showed in Fig. 3 and S2 further confirmed the presence of aldehyde groups, showing a C=O stretching band at 1725 cm^{-1} and a signal at 2842 cm^{-1} corresponding to the sp^2 C–H bond of the aldehyde groups (Fig. 3).[24] These results indicated that HAD, an aldehyde-containing hyaluronic acid was successfully synthesized by periodate oxidation.

ACD was synthesized through a two steps reaction. First, the hydroxyl groups of β-cyclodextrin (bCD) were activated using tosyl chloride (TsCl), followed by coupling with ethylenediamine (EDA), as shown in Fig. 1b. The ^{1}H-NMR spectrum of bCDTS displayed aromatic proton signals at 7.43–7.77 ppm. These signals disappeared when tosyl groups were substituted by ethylenediamine (EDA), providing the formation of ACD. The ^{1}H-NMR spectrum of ACD (Fig. 2 and S3) exhibited new signals at 2.66–2.98 ppm, corresponding to the ethylene moiety attached to bCD, while signals at 4.95 ppm were assigned to the anomeric protons of b-CD, while signals at 3.47–3.87 ppm corresponded to protons of the glucopyranose units of bCD. The FT-IR spectrum of ACD showed an O–H stretching absorption peak at 3302 cm^{-1}, along with an N–H bending vibration at 1641 cm^{-1} (Fig. 3).[38] These results confirm the successful synthesis of ACD.

3.2 Fabrication of hydrogels

HAD/ACD/HACC hydrogels were fabricated by first mixing HAD and ACD solution, followed by the addition of HACC solution, and adjusting the pH to neutral by using PBS pH 7.4. As shown in Fig. 1d, HAD contains aldehyde groups, while ACD has amino groups; therefore, they can react to form a Schiff base linkage. The formation of hydrogels was facilitated by the addition of HACC, which contains multiple positive charges of the ammonium moiety and retains some free amino groups at pH 7.4. This allows for intermolecular ionic interaction between the negative charge of the carboxylate groups of HAD and the positively charged HACC, stabilizing the hydrogel structure. Simultaneously, the remaining amino groups of HACC could also form additional Schiff base linkages with the unreacted aldehyde groups of HAD, further enhancing hydrogel stabilization. Moreover, in the absence of ACD, hydrogels cannot form, suggesting that ACD not only forms Schiff base linkage with HAD but also contributes hydrogen bonding with HACC to create a stable hydrogel network. The different ratios of HAD:ACD:HACC used for hydrogel formation are shown in Table 2. Hydrogel constructed with low molecular weight HAD (10k) could not form, whereas the hydrogel formed with higher molecular weight HAD showed more stability.

Table 1 Percent yield and oxidation degree of HAD synthesis with various molecular weights, amounts of $NaIO_4$, and reaction times

M_w HA (kDa)	Eq. $NaIO_4$	Reaction time (h)	% Yield	Oxidation degree (% OD)
10	0.5	24	24	49
10	2.0	24	40	95
100	0.5	2	96	27
100	0.5	4	96	66
100	0.5	24	84	74
100	2.0	24	66	88
1000	2.0	24	40	84
1000	2.0	24	50	92
2000	0.5	24	59	62
2000	2.0	24	70	90

The formation of the Schiff base was investigated using ^{1}H-NMR (Fig. 2). The results showed that imine protons appeared at 8.37 and 9.12 ppm for both the HAD/ACD mixture and the HAD/ACD/HACC hydrogel in D_2O. Moreover, the signals corresponding to the hemiacetal groups of HAD disappeared. The FTIR spectrum of HAD-ACD-HACC (Fig. 3) showed new absorption signals for Schiff base (imine bond, C=N) at 1649 and 1559 cm^{-1}, including the sp^2 C–H stretching peaks at 2842 cm^{-1}, which disappeared, indicating that Schiff base formation occurred between HAD and either ACD or HACC. These results fully demonstrate that the Schiff base reaction occurred between –NH_2 of ACD and –CHO of HAD.

3.3 Morphologies, self-healing property, and swelling ratio of HAD/ACD/HACC hydrogels

The morphology of lyophilized HAD/ACD/HACC hydrogels was investigated using SEM (Fig. 4a and b). The SEM images of the hydrogels' cross-sections revealed a three-dimensional interconnected porous structure with varying pore sizes. This porous structure provides the hydrogel with excellent swelling capacity and facilitates the loading of drug molecules into its cavities. The pore size of all hydrogels was determined using ImageJ software and is shown in Fig. 5. In this system, crosslinking occurred through the formation of imine bonds and interactions between the positively charged HACC and the negatively charged carboxyl groups of HAD. With an increase in HAD content, the crosslinking degree of hydrogels also increased. A higher crosslinking density resulted in the formation of denser network structures, as observed in hydrogels 1M-2 and 2M-2. Hydrogel 10k-1 and 10k-2 displayed the smallest pore size due to the low molecular weight of HAD, which led to reduced crosslinking processes.

Fig. 4b and c showed hydrogels were formed within 15 min by triggering the Schiff base reaction *via* mixing the HAD and ACD solution with and without Que first, then the HACC solution was added into the mixture at room temperature. In addition, the self-healing property of hydrogels was studied using two different dyed hydrogels combined at room temperature (Fig. 4d). After 30 min of contact, two different colors of hydrogel formed self-healed. It maintained its strength and completeness after 2 h. The self-healing mechanism of HAD-ACD-HACC hydrogels was that the dynamic imine bond could be spontaneously reformed through the Schiff base reaction at room temperature.

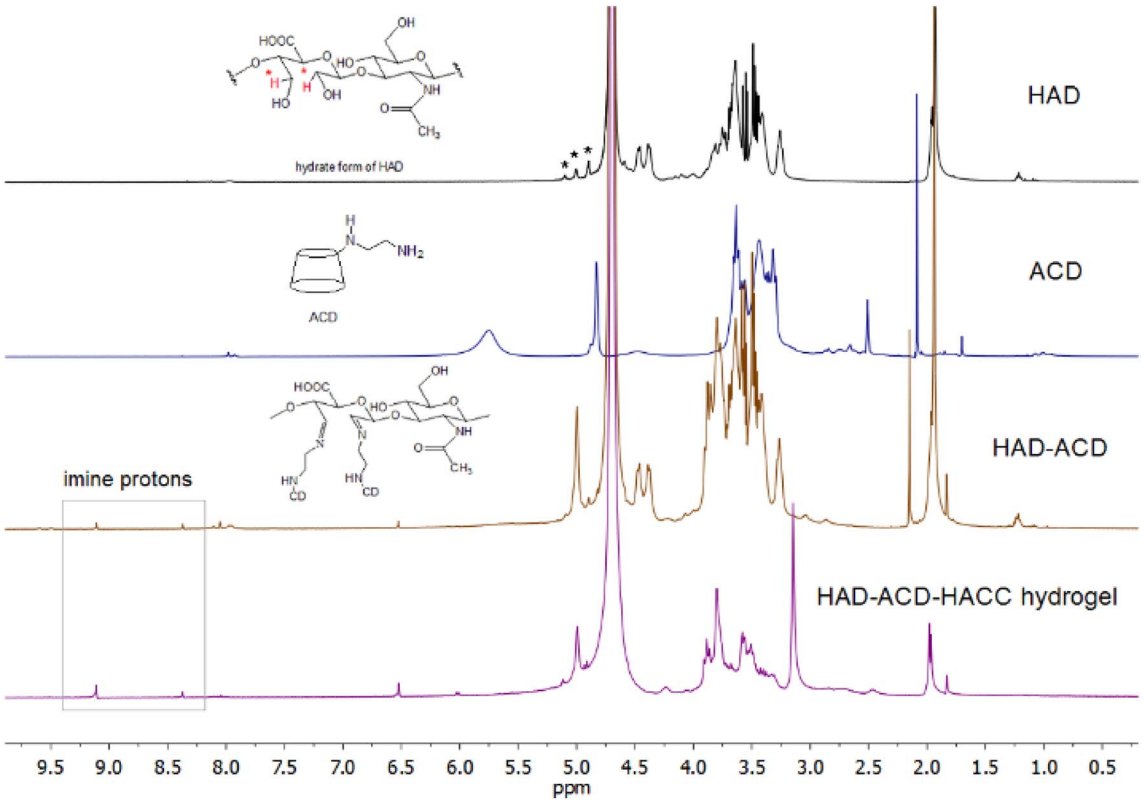

Fig. 2 ^{1}H-NMR spectra of HAD, ACD, HAD-ACD, and 100k-2 hydrogel.

The water swelling capacity of the hydrogels was evaluated by determining of the swelling ratio (Fig. 5). The results showed the swelling ratio of all hydrogels in water at room temperature. Hydrogels containing a higher amount of HAD (10k-2, 100k-2, 1M-2 and 2M-2) exhibited greater swelling compared to hydrogels with a lower HAD content (10k-1, 100k-1, 1M-1, and 2M-1).

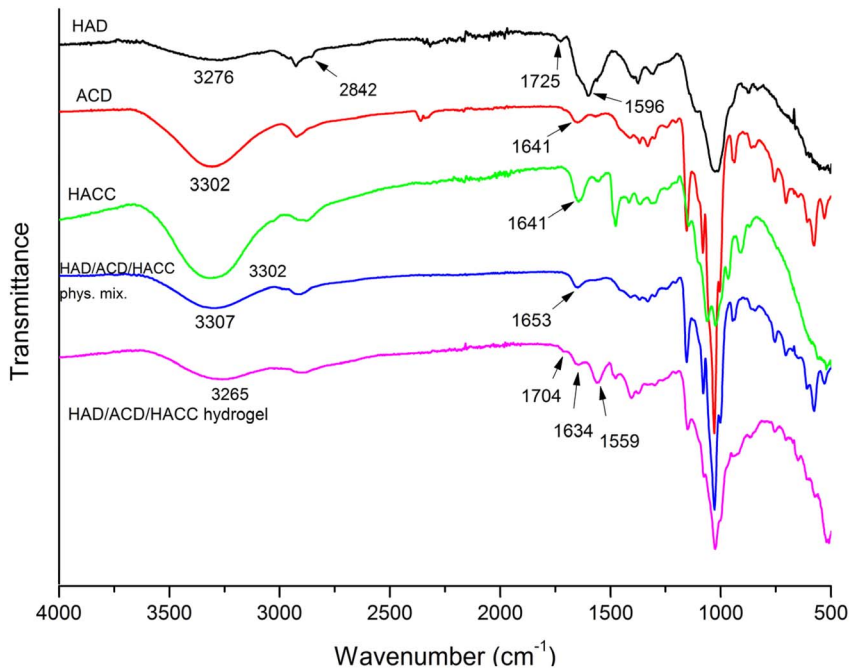

Fig. 3 FT-IR spectra of HAD, ACD, HACC, physical mixture of HAD-ACD-HACC, and 100k-2 hydrogel.

Table 2 The content of HAD, ACD, and HACC in various formulation of hydrogels

Gels	M_w of HAD (kDa)	Molar ratio HAD	ACD	HACC	Observation
10k-1	10	1	2	10	Fluid gel degraded in 1 h
10k-2	10	2	2	10	Fluid gel degraded in 2 h
100k-1	100	1	2	10	Stiff gel
100k-2	100	2	2	10	Gel
1M-1	1000	1	2	10	Stiff gel
1M-2	1000	2	2	10	Gel
2M-1	2000	1	2	10	Stiff gel
2M-2	2000	2	2	10	Gel

This is because a higher HAD content leads to more crosslinking, as well as a larger number of hydrophilic groups, which can absorb large amounts of water. Additionally, the three-dimensional network structure facilitates the easy entry of free water. However, hydrogels containing a higher molecular weight of HAD demonstrated greater water absorption capacity than those made from a lower molecular weight of HAD. These results correlated with the average pore size of the hydrogels described above.[39] Hydrogels with larger pores and a greater number of hydrophilic functional groups swelled to a greater extent and absorbed more water than gels with smaller pore sizes.[40,41]

3.4 Rheological properties of HAD/ACD/HACC hydrogels

The storage modulus (G') and loss modulus (G'') of the hydrogels were measured using a rheometer (Fig. 6A). Five hydrogels 1M-1, 1M-2, 2M-1, 2M-2 and 100k-2 remained stable at room temperature for more than three days. In contrast, hydrogels made from low molecular weight HAD (10k-1 and 10k-2) and 100k-1 with lower HAD content were degraded within an hour, making it impossible to study their rheological properties. All five selected hydrogels exhibited higher G' (indicating elastic behavior) than G'' (indicating viscous behavior) values, demonstrating their high elasticity. When the strain increased, the G' curve sloped down and then intersected with the G'' curve, indicating that hydrogel's network collapse. Increasing the HAD content to two equivalents (1M-2) compared to one equivalent of HAD (1M-1) improved the hydrogel's elasticity properties due to enhanced crosslinking processes. Hydrogel 2M-2 showed the highest G' value, indicating an optimal crosslinked network structure that resulted in high elasticity, similar to 2M-2 and 100k-2 hydrogels. In the case of 1M-1, the crosslinking structure was too stiff and too flexible, leading to lower elasticity, as indicated by its lower G' values. However, this formulation exhibited the highest elastic modulus at strain of 120%. The G' value of 100k-2 was closest to that of native human vitreous ($G' \sim 100$ Pa).[22] These results correlated with the pore sizes and swelling ratios of hydrogels where hydrogels with small pores exhibited lower water absorption capacity and elasticity property. The 1M-2 and 100k-2 formulations appeared to have a suitable ratio of aldehyde groups crosslinked with the amino group of ACD and HACC, forming a stable three-dimension hydrogel network; thus, these two formulations were used for further quercetin encapsulation and release study.

The self-healing property of hydrogels can be quantified by stress–strain scanning.[42] Three hydrogels, 100k-2, 1M-2 and 2M-

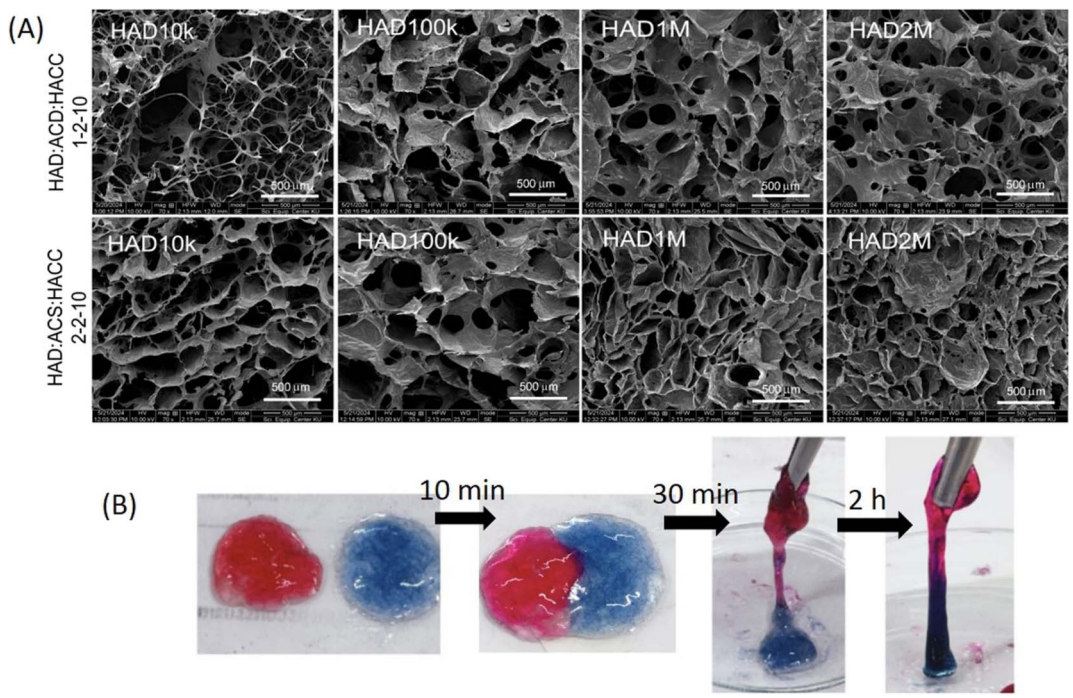

Fig. 4 The morphology of hydrogels. (A) SEM images of hydrogels (10k-1, 100k-1, 1M-1, 2M-1, 10k-2, 100k-2, 1M-2 and 2M-2 respectively); (B) visual observation of hydrogel formation for 100k-2 (top) and Q100k-2 (bottom) gelling solution.

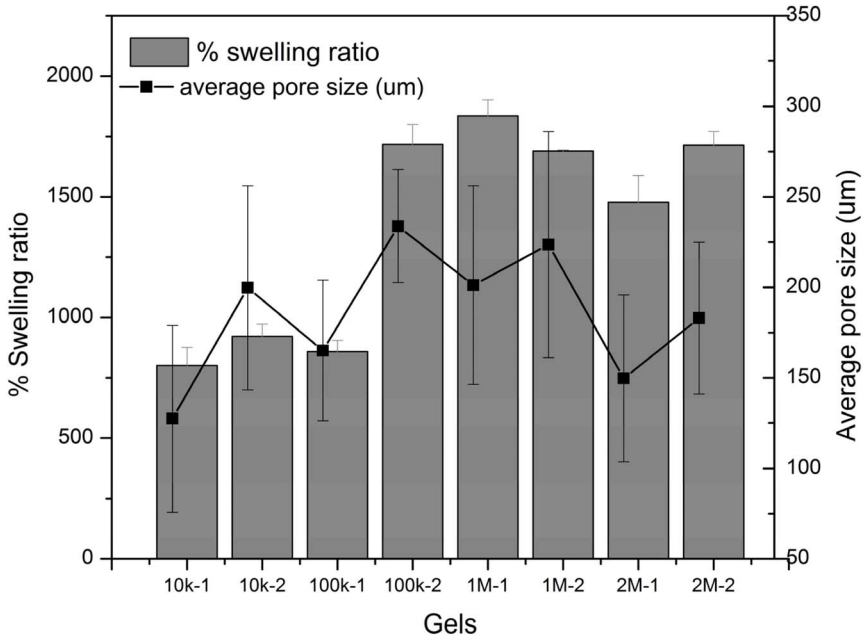

Fig. 5 The swelling ratio (bar) and pore size (line) of all hydrogels.

2 were selected to investigate because of their high G' (Fig. 6B). A lower strain (1%) is applied to hydrogels, with G' greater than G'', indicating that the hydrogels are within the elastic range. When a high strain (150%) is applied to hydrogels, G' is lower than G'', indicating hydrogel network collapse. After 300 seconds of self-healing, the G' and G'' return to the pre-fracture state. Even after three cycles of repetition, their values almost return to original levels. These results confirm the self-healing property of HAD-ACD-HACC hydrogels.

3.5 Drug loading and release studies

The quercetin loaded in hydrogel 1M-2 (Q1M-2) and 100k-2 (Q100k-2) were selected due to the stability of the hydrogels. These hydrogels were prepared using the quercetin:ACD (Que:ACD) inclusion complex in place of ACD in the same concentration as blank hydrogels. The Que:ACD inclusion complex was characterized using ^{1}H-NMR and UV-Vis spectrometry (Fig. S4 and S5, SI). The ^{1}H-NMR spectra of Que:ACD inclusion complex show aromatic protons of quercetin at 6.82–8.38 ppm. The UV-Vis absorption spectra exhibited a blue shift of the maximum absorption (λ_{max}) from 390 to 335 nm, which implies that quercetin was encapsulated within the ACD cavity, which is a hydrophobic environment. Moreover, the stoichiometry of Que : ACD was studied using Job's plot, which indicated a 1 : 1 ratio (data shown in SI, Fig. S6).[43] The loading capacity (% LC) of quercetin in ACD inclusion complex was 66.36 ± 2.13%. The encapsulation efficiency (% EE) of quercetin in the 1M-2 and 100k-2 hydrogels was 98.42 ± 1.48% and 99.35 ± 2.04%, respectively.

An *in vitro* release study was conducted by adding quercetin-loaded hydrogel into solution in PBS pH 5 and 7.4 at 37 °C. The results, shown in Fig. 7, indicated that quercetin was detected in the PBS solution, suggesting that the Schiff base linkages in the hydrogel were hydrolyzed, allowing the quercetin:ACD inclusion complex to slowly diffuse through the three-dimensional network. Quercetin was released more rapidly from hydrogel 1M-2 than from 100k-2. According to the results, SEM images revealed that the crosslink density in hydrogel 1M-2 was higher than in 100k-2. This suggested that the contact surface area of hydrogel 1M-2 with water was greater than that of hydrogel 100k-2. This indicates that the contact surface area of hydrogel 1M-2 with water was greater than that of hydrogel 100k-2, leading to faster degradation of the imine bond in hydrogel 1M-2. Furthermore, quercetin releases faster at lower pH (pH 5), than at higher pH (pH 7.4), likely due to the hydrolysis of imine linkage occurring in acidic conditions.[44] Moreover, at pH 7.4, quercetin release was influenced by the neutralization of amino groups ($-NH_2$) in HACC, while the carboxyl groups of HAD were deprotonated, forming negative charge COO^- ions. This increased intermolecular electrostatic repulsion, led to the breakdown of the hydrogel network, facilitating the release of quercetin.

3.6 Cell viability

To evaluate the probable effects of pure quercetin (Que) on HaCaT cells, the standard WST-1 assay was performed to investigate the cell viability in HaCaT cells after exposure to Que at six concentrations (80–1250 μg mL^{-1}). The results showed that cell viability remained above 80% at concentrations up to 1250 μg mL^{-1} after a 24-h. incubation period (Fig. 8a). To certify the cytotoxic effects, quercetin-loaded 100k-2 hydrogel (Q100k-2) and blank 100k-2 hydrogel were also tested on HaCaT cells (Fig. 8b and c). At maximum concentration, Q100k-2 and 100k-2 showed approximately 30% inhibition of cell proliferation. According to the WST-1 assay results, a concentration threshold was established to ensure cell viability above 80%. For

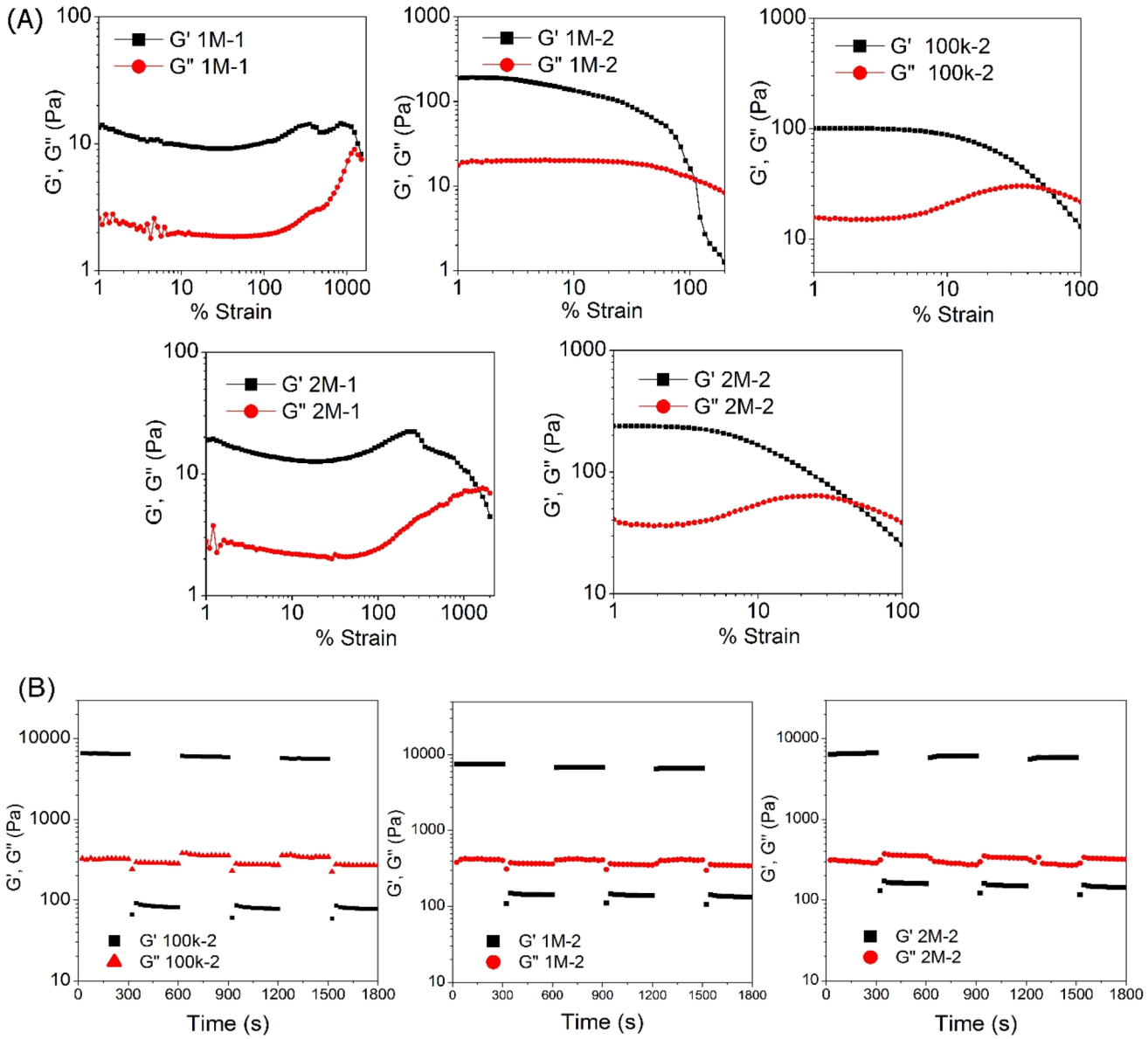

Fig. 6 The rheological studies of hydrogels: (A) strain sweep of hydrogels 1M-1, 1M-2, 2M-1, 2M-2, and 100k-2 at 37 °C. (B) Alternate step strain switch from 1% and 150% strain of 100k-2, 1M-2, and 1M-2 hydrogels.

subsequent experiments, Que was used at 160 μg mL^{-1}, while 100k-2 and Q100k-2 were used at 100 μg mL^{-1} to prevent any cytotoxic effects on HaCaT cell lines for the rest of the experiments.

3.7 Inflammatory cytokine levels study

Stimuli that induce inflammation in keratinocytes include ultraviolet B (UVB), interleukin (IL)-1α, lipopolysaccharide (LPS), tumor necrosis factor alpha (TNF-α), and interferon gamma (IFN-γ). The activated keratinocytes produce inflammatory cytokines such as TNF-α, IL-1, IL-6, IL-8, IL-10 and IFN-γ, along with other inflammatory mediators including nitric oxide (NO) and prostaglandin E2 (PGE2) which contribute to the inflammatory response in the skin. In an anti-inflammatory study, the levels of TNF-α, IL-6, IL-10, and PEG2 were measured to evaluate the anti-inflammatory activity. The inhibitory effects of Que and quercetin-loaded 100k-2 hydrogel (Q100k-2) on inflammatory cytokine levels were investigated in HaCaT human keratinocytes. After treatment with Que and Q100k-2, HaCaT cells were stimulated by exposure to UVA/UVB. The inflammatory cytokine/mediator levels are shown in Fig. 9. Both D,L-1′-acetoxychavicol acetate (DL-1) and beta-glucan (β-glucan) were used as standards. Compared to the non-UV-treated control, UV-treaded cells exhibited significantly higher levels of inflammatory cytokines/mediators (Fig. 9). The results demonstrated that Que treatment effectively inhibited the production of inflammatory cytokines, with TNF-α levels at 423.47 ± 2.08 pg mL^{-1}, IL-6 at 100.97 ± 1.04 pg mL^{-1}, and PGE2 at 168.46 ± 2.69 pg mL^{-1}. Similarly, Q100k-2 significantly reduced inflammatory cytokine levels to 163.16 ± 3.64 pg mL^{-1}

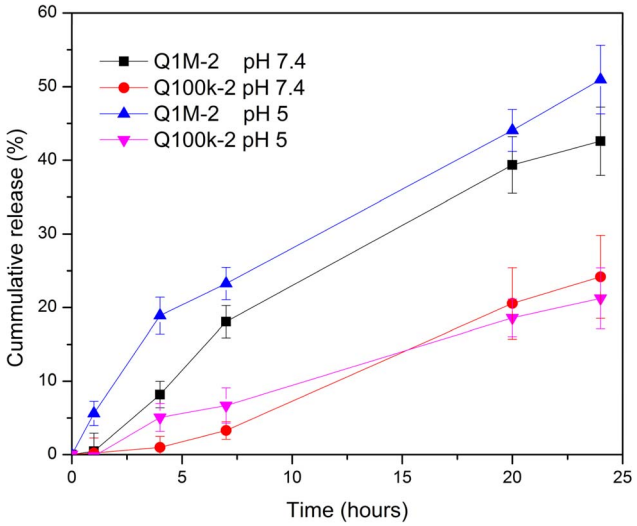

Fig. 7 Cumulative release of quercetin from Q100K-2 and Q1M-2 hydrogel in PBS 5 and pH 7.4 during 24 h.

for TNF-α, 47.70 ± 0.39 pg mL^{-1} for IL-6, and 83.63 ± 1.34 pg mL^{-1} for PGE2 compared to the UV-induced control group. Moreover, the production of IL-10, a key cytokine involved in preventing inflammation, increased significantly after treatment with Que and Q100k-2, reaching 57.53 ± 1.45 pg mL^{-1} and 71.87 ± 0.58 pg mL^{-1}, respectively, compared to non-UV-treated cells controls. These findings suggest that the inclusion complex of ACD and quercetin effectively reduces the production of pro-inflammatory cytokines in cells, as well as enhances the IL-10 level, which plays a crucial role in suppressing inflammatory. The encapsulation of quercetin in HAD-ACD-HACC hydrogel likely improved its solubility, contributing to the reduction of TNF-α, IL-6, and PGE2 secretion while promoting IL-10 production. However, when the blank hydrogel (100k-2) without quercetin was tested, it did not exhibit any significantly reduction in TNF-α, IL-6, or PGE2 levels, nor did it enhance IL-10 production. This confirms that the observed anti-inflammatory effects were primarily attributed to the presence of quercetin in the hydrogel system.

3.8 Scratch-wound healing assay

The *in vitro* scratch wound model is commonly used to examine cell migration and wound closure.[45] The migration effect of HaCaT cells after incubation with various treatment groups was evaluated at 24, 48 and 72 hous (Fig. 9A). The results indicated that the Q1M-2 and Q100k-2 gels significantly enhanced HaCaT migration from scratch's edge in comparison to the control group. Quantitative analysis of the scratch area revealed that the Q1M-2 gel and Q100k-2 hydrogels achieved complete (100%) wound closure at 24 and 48 h, respectively whereas the control group reached 100% closure at 72 hours (Fig. 9B). These

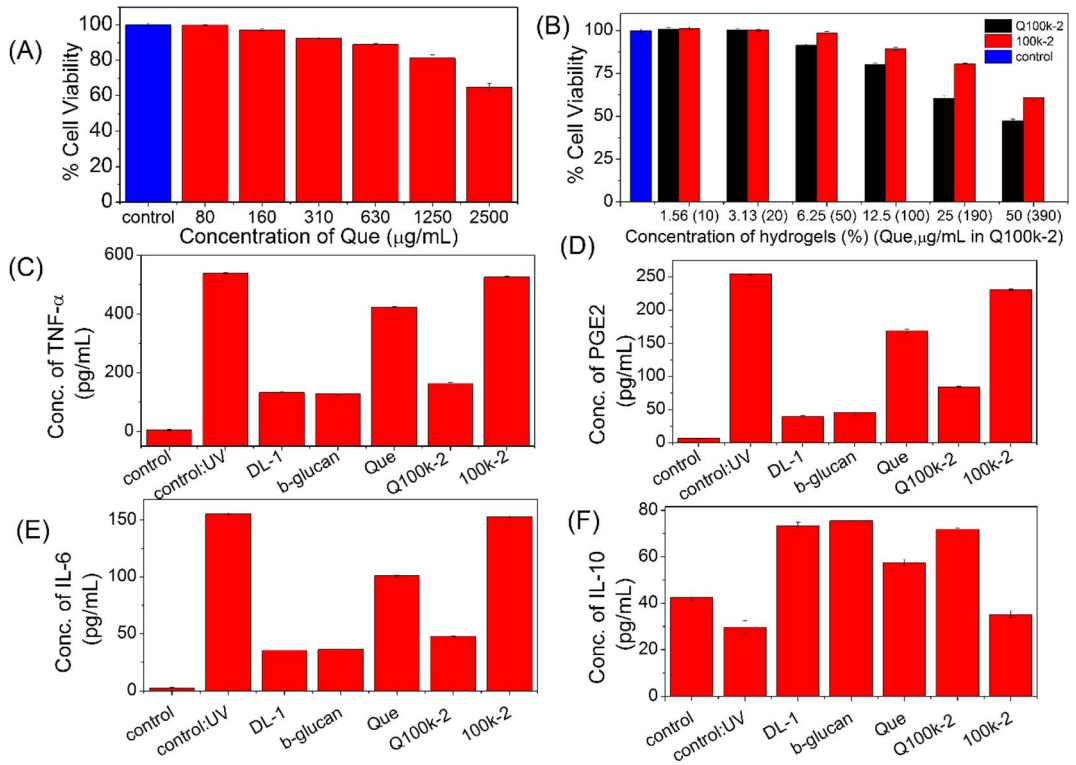

Fig. 8 Effect of (A) Que, (B) Q100k-2 and 100k-2 on HaCaT cell viability, as assayed by the WST-1 assay. The data were normalized by setting 100% equal to the viability of the untreated control group. Error bars indicate the standard deviation of the mean among the three replications in each treatment group. Concentration of inflammatory cytokines (C) TNF-α, (D) IL-6, (E) PGE2 and (F) IL-10 against Que, Q100k-2, and 100k-2 (gel blank).

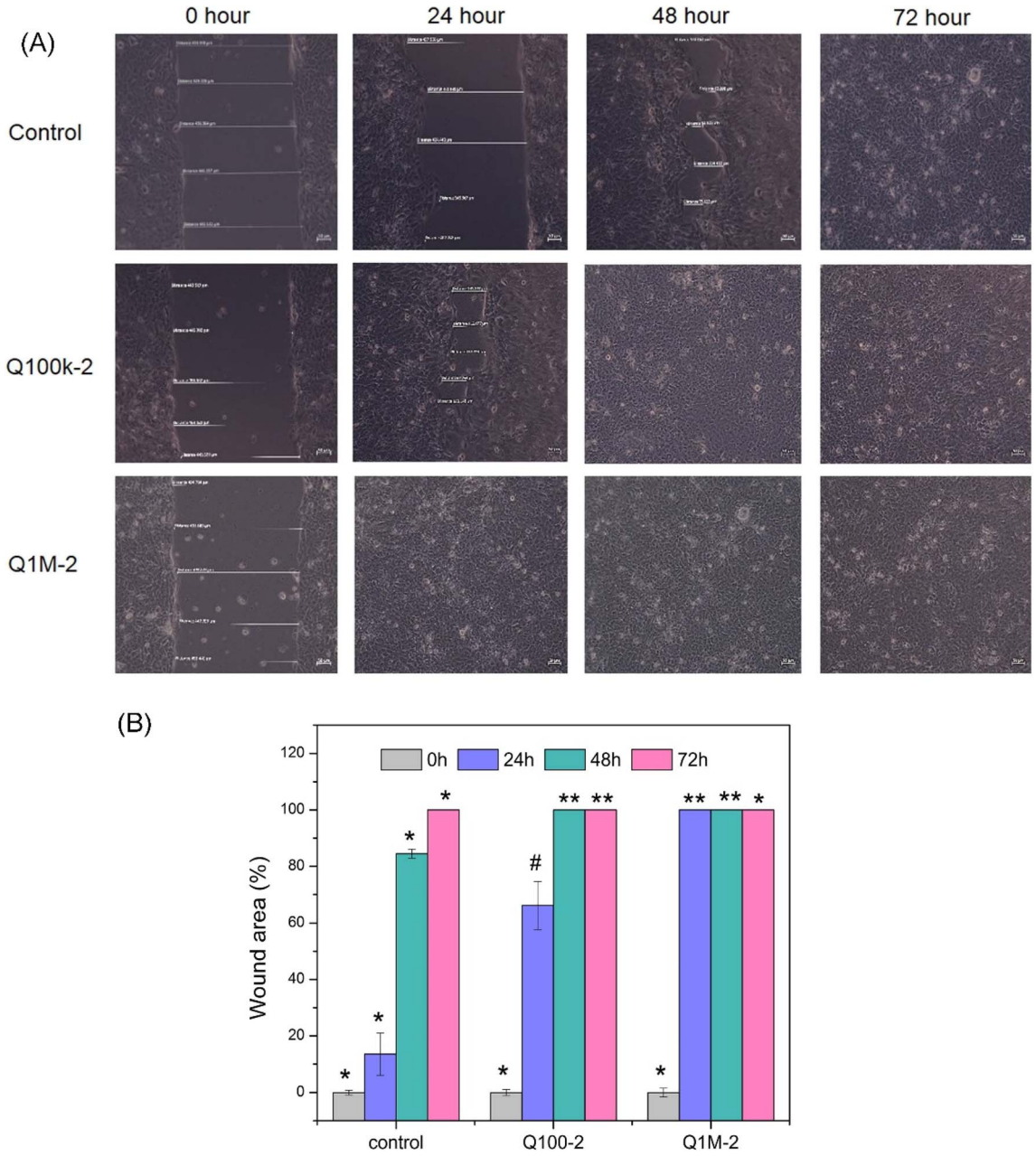

Fig. 9 Scratch-wound healing assay. (A) The microscopy images of HaCaT migration after 24, 48 and 72 h treated with 12.5 mg per mL Q100k-2 and Q1M-2 hydrogels. (B) The quantification result of the wound area (%). *, ** and # significant different from control at $P < 0.05$.

findings clearly demonstrate the superior efficacy of quercetin loaded HAD-ACD-HACC hydrogels in accelerating wound healing, reinforcing their potential as an advanced wound dressing materials.

4. Conclusions

In this study, hydrogels based on hyaluronic acid were successfully prepared using hyaluronic dialdehyde (HAD) and amino-β-cyclodextrin (ACD) *via* Schiff base linkage, with the incorporation of quaternary ammonium chitosan (HACC). The developed hydrogel system was rationally designed to address the major limitations of quercetin for biomedical applications, particularly its poor water solubility and rapid clearance. ACD was employed to form an inclusion complex with quercetin, thereby significantly enhancing its aqueous solubility through host–guest interactions. In our system, ACD also serves as a reactive site for Schiff base formation with the hyaluronic acid dialdehyde (HAD), enabling covalent crosslinking and integration into a hydrogel network. The use of hyaluronic acid as a backbone not only provides biocompatibility and biodegradability but also allows tuning of the hydrogel's physical properties by varying its molecular weight. The crosslinked network effectively retains the Que:ACD complex, allowing for controlled

and prolonged release in various pH media. Additionally, the incorporation of cationic chitosan (HACC) contributes to enhanced electrostatic interactions and stabilization of the hydrogel structure. Importantly, the enhanced solubility and sustained delivery of quercetin from the hydrogel system improved its anti-inflammatory activity compared to free quercetin. In our *in vitro* study, HaCaT cells treated with quercetin-loaded hydrogel exhibited significantly greater inhibition of pro-inflammatory cytokines than those treated with a more equivalent dose of pure quercetin, and also enhanced wound healing property. This improvement can be attributed to the higher local concentration, better cellular uptake, and prolonged exposure provided by the hydrogel matrix. These findings suggest that the developed hydrogels have strong potential as a novel drug delivery system.

Author contributions

Parichat Sutthisawatkul: writing original draft, investigation, and data curation. Kanyalux Stapornpiriyadaj: investigation, and formal analysis. Onuma Mongkhon: investigation, and formal analysis. Weerasak Taengphan: investigation, and formal analysis. Theerachart Leepasert: investigation, and formal analysis. Thitinun Karpkird: writing – review and editing, supervision, project administration, and funding acquisition.

Conflicts of interest

The authors declare no competing financial interest.

Data availability

The data supporting this article have been included as part of the SI. See DOI: **https://doi.org/10.1039/d5ra03329b**.

Acknowledgements

This research is funded by Kasetsart University Research and Development Institute, KURDI (FF(KU) 50.68) and Kasetsart University through the Graduate School Fellowship Program.

References

1 L. G. Costa, J. Garrick, P. J. Roque and C. Pellacani, *Nutraceuticals in CNS Diseases: Potential Mechanisms of Neuroprotection*, Elsevier Inc., 2016.
2 E. Safarzadeh, S. Ataei, M. Akbari, R. Abolhasani, M. Baziar, V. Asghari-Azar and M. Dadkhah, *Exp. Gerontol.*, 2024, **193**, 112466.
3 M. Marina, A. R. Nevena, S. V. Zorica, B. Biljana, V. Dragana and J. Ivan, *J. Pharm. Pharm. Sci.*, 2010, **13**, 311–319.
4 B. Parhi, D. Bharatiya and S. K. Swain, *Saudi Pharm. J.*, 2020, **28**, 1719–1732.
5 P. Lv, P. Han, Y. Cui, Q. Chen and W. Cao, *Immun., Inflammation Dis.*, 2024, **12**, 1–8.
6 S. Pruksawan, Z. A. Chua, Y. T. Chong, T. J. E. Loh, E. L. L. Ng and F. K. Wang, *ACS Appl. Polym. Mater.*, 2024, **6**, 12362–12381.
7 P. Tithayanu, *Phytother Res.*, 2009, **22**, 557–559.
8 R. Solanki, D. Bhatia, R. Solanki and D. Bhatia, *Gels*, 2024, **10**, 440.
9 S. Mitura, A. Sionkowska and A. Jaiswal, *J. Mater. Sci. Mater. Med.*, 2020, **31**(50), 1–14.
10 L. Chen and S. A. Khan, *RSC Pharm.*, 2024, **1**, 689–704.
11 M. Z. Quazi and N. Park, *Biomacromolecules*, 2023, **24**, 2127–2137.
12 S. Cascone and G. Lamberti, *Int. J. Pharm.*, 2020, **573**, 118803.
13 J. Manasi Esther, R. Solanki, M. Dhanka, P. Thareja and D. Bhatia, *Mater. Adv.*, 2024, **5**, 5365–5393.
14 K. J. Wolf and S. Kumar, *ACS Biomater. Sci. Eng.*, 2019, **5**, 3753–3765.
15 G. D. Prestwich, *J. Contr. Release*, 2011, **155**, 193–199.
16 M. P. Sekar, S. Suresh, A. Zennifer, S. Sethuraman and D. Sundaramurthi, *ACS Biomater. Sci. Eng.*, 2023, **9**, 3134–3159.
17 Y. Liu, M. Hao, Z. Chen, L. Liu, Y. Liu, W. Yang and S. Ramakrishna, *Curr. Opin. Biomed. Eng.*, 2020, **13**, 174–189.
18 H. Yang, L. Song, Y. Zou, D. Sun, L. Wang, Z. Yu and J. Guo, *ACS Appl. Bio Mater.*, 2021, **4**, 311–324.
19 N. Samiraninezhad, K. Asadi, H. Rezazadeh and A. Gholami, *Int. J. Biol. Macromol.*, 2023, **252**, 126573.
20 Y. Lin, J. Xu, Y. Dong, Y. Wang, C. Yu, Y. Li, C. Zhang, Q. Chen, S. Chen and Q. Peng, *Carbohydr. Polym.*, 2023, **314**, 120962.
21 H. J. Prado and M. C. Matulewicz, *Eur. Polym. J.*, 2014, **52**, 53–75.
22 W. Wang, D. Shi, Y. Zhang, W. Li, F. Li, H. Feng, L. Ma, C. Yang, Z. Peng, G. Song, H. Zeng and L. Xie, *Int. J. Biol. Macromol.*, 2023, **245**, 125341.
23 F. Zhang, S. Zhang, R. Lin, S. Cui, X. Jing and S. Coseri, *Int. J. Biol. Macromol.*, 2023, **249**, 125801.
24 S. Li, Q. Dong, X. Peng, Y. Chen, H. Yang, W. Xu, Y. Zhao, P. Xiao and Y. Zhou, *ACS Nano*, 2022, **16**, 11346–11359.
25 Y. Yue, Y. Liu, Y. Lin, F. Guo, K. Cai, S. Chen, W. Zhang and S. Tang, *Int. J. Biol. Macromol.*, 2024, **257**, 128534.
26 H. Weng, W. Jia, M. Li and Z. Chen, *Carbohydr. Polym.*, 2022, **294**, 119767.
27 S. Daoud-Mahammed, P. Couvreur, K. Bouchemal, M. Chéron, G. Lebas, C. Amiel and R. Gref, *Biomacromolecules*, 2009, **10**, 547–554.
28 K. Mai, S. Zhang, B. Liang, C. Gao, W. Du and L. M. Zhang, *Carbohydr. Polym.*, 2015, **123**, 237–245.
29 Z. Fülöp, T. T. Nielsen, K. L. Larsen and T. Loftsson, *Carbohydr. Polym.*, 2013, **97**, 635–642.
30 S. Sakulwech, N. Lourith, M. Kanlayavattanakul, S. Phunpee, K. Suktham, S. Surassmo and U. R. Ruktanonchai, *Colloids Surf., B*, 2022, **220**, 112920.
31 Y. Kim, Y. Hu, J. pil Jeong and S. Jung, *Carbohydr. Polym.*, 2022, **284**, 119195.
32 Y. Shin, Y. Hu, S. Park and S. Jung, *Carbohydr. Polym.*, 2023, **305**, 120568.

33 L. Chen, Q. Dong, Q. Shi, Y. Du, Q. Zeng, Y. Zhao and J. J. Wang, *Biomacromolecules*, 2021, **22**, 2790–2801.
34 C. Lou, X. Tian, H. Deng, Y. Wang and X. Jiang, *Carbohydr. Polym.*, 2020, **231**, 115678.
35 R. R. Vildanova, N. N. Sigaeva, O. S. Kukovinets and S. V. Kolesov, *Polym. Test.*, 2021, **96**, 107120.
36 Y. Li, H. Guo, Y. Zhang, J. Zheng, Z. Li, C. Yang and M. Lu, *Carbohydr. Polym.*, 2014, **102**, 278–287.
37 Z. Li, H. Liu, C. Qi, A. Yang and S. Deng, *J. Inclusion Phenom. Macrocyclic Chem.*, 2019, **93**, 289–299.
38 L. Yuan, Z. Li, X. Li, S. Qiu, J. Lei, D. Li, C. Mu and L. Ge, *ACS Appl. Polym. Mater.*, 2022, **4**, 1243–1254.
39 Y. Wang, Y. Chen, J. Zheng, L. Liu and Q. Zhang, *ACS Omega*, 2022, **7**, 12076–12088.
40 X. Zhong, C. Ji, A. K. L. Chan, S. G. Kazarian, A. Ruys and F. Dehghani, *J. Mater. Sci. Mater. Med.*, 2011, **22**, 279–288.
41 Y. Yi, X. Wang, Z. Liu, C. Gao, P. Fatehi, S. Wang and F. Kong, *J. Appl. Polym. Sci.*, 2022, **139**, 1–10.
42 J. Karvinen and M. Kellomäki, *Eur. Polym. J.*, 2022, **181**, 111641.
43 P. Job, *Ann. Chim.*, 1928, **9**, 113.
44 M. Skrt, P. Mrak, D. Komes and P. Ulrih, *Food Chem.*, 2024, **459**, 140347.
45 J. E. N. Jonkman, J. A. Cathcart, F. Xu, M. E. Bartolini, J. E. Amon, K. M. Stevens and P. Colarusso, *Cell Adhes. Migr.*, 2014, **8**, 440–451.